Coordinated Control of Wind Energy Conversion Systems for Mitigating Subsynchronous Interaction in DFIG-Based Wind Farms

Ulas Karaagac, *Member, IEEE*, Sherif O. Faried, *Senior Member, IEEE,* Jean Mahseredjian, *Fellow, IEEE,* and Abdel-Aty (Aty) Edris, *Fellow, IEEE*

***Abstract*—The paper presents methods for mitigating subsynchronous interaction (SSI) between doubly fed induction generator (DFIG) based wind farms and series capacitor compensated transmission systems. SSI damping is achieved by introducing a supplemental control signal in the reactive power control loop of the grid side converter of DFIG and full-scale frequency converter wind turbines, as well as in the reactive power control loop of the HVDC onshore multimodule converter (MMC) of offshore wind farms. This paper also investigates the impact of the phase imbalance series capacitive compensation concept that was introduced in the 1990s as a subsynchronous resonance countermeasure on SSI damping. The validity and effectiveness of the proposed methods are demonstrated on a test benchmark through time domain simulation studies using the ElectroMagnetic Transient Program (EMTP-RV).**

***Index Terms*—Doubly-fed induction generator, phase imbalance, series capacitor compensation, subsynchronous interaction, voltage-source converters, wind energy.**

I. Introduction

Recent studies have identified the vulnerability of doubly fed induction generator (DFIG) wind turbines to subsynchronous resonance interaction (SSI) [1], [2]. This was confirmed in October 2009 by the Zorillo Gulf wind farm incident in Texas, which can be regarded as the first event of SSI between a DFIG-based wind farm (485 MW) and a series capacitor compensated transmission line (345 kV, 80 miles and a 50% compensation degree) [3]–[5]. As most large wind farms in Europe and North America employ DFIG wind turbines, there has recently been a growing interest in developing effective and practical SSI mitigation methods [6]–[10].

The use of static var compensator (SVC) to damp SSI is presented in [6], where the studies were conducted on a simple system consisting of a DFIG-based wind farm connected via a transformer to an infinite-bus system through a series capacitor compensated transmission line. Linearization techniques, eigenvalue, and residue-based analyses were used in the studies reported in [1] and [7] for studying SSI and the design of a supplemental control for the grid side converter of the DFIG-wind turbines. However, a simple system similar to that reported in [6] was used in these studies and SSI was observed at the unrealistic compensation levels (70% compensation degrees and/or higher). It worth noting here that transmission lines with fixed series capacitors and 60% compensation degree or higher do not exist. Practical fixed series capacitor compensation degrees are 55% or less. It should be also noted that the linearization techniques and eigenvalue analysis are valid only for small perturbations. In practice, the necessary conditions for SSI can be expected to occur following a large disturbance that causes a major change in electrical network such as loss of a line or a busbar following a fault. Therefore, the system nonlinearities (such as magnetic saturation of generators, limiters in controls) should be considered while investigating SSI and testing the performance of the proposed countermeasures. Moreover, these techniques are quite difficult to be performed on large systems comprising several voltage-sourced converter back-to-back (BtB) links. Therefore, transient time analysis is the most appropriate tool for studying SSI as it enables detailed modeling of machines, system controllers, switching devices and transient faults.

This paper presents methods for damping SSI in DFIG-based wind farms connected to series capacitor compensated transmission systems. SSI damping is achieved by introducing a supplemental control signal in the reactive power control loop of the grid side converter of DFIG and full-scale frequency converter (FFC) wind turbines as well as in the reactive power control loop of the HVDC onshore modular multilevel converter (MMC) of offshore wind farms. The paper investigates also the impact of phase imbalance series capacitive compensation concept that was introduced in the 1990s as a subsynchronous resonance (SSR) countermeasure on SSI damping. The validity and effectiveness of the proposed SSI mitigation methods are demonstrated on a test benchmark through time domain simulation studies using the EMTP-RV.

II. System Under Study

To evaluate the effectiveness of the proposed SSI mitigation methods, the system shown in Fig. 1 is adopted as a test benchmark. It consists of four wind farms designated as wind farms

Manuscript received May 11, 2013; revised October 7, 2013, January 5, 2014, February 28, 2014, and April 26, 2014; accepted June 10, 2014. Paper no. TSG-00373-2013.

U. Karaagac and J. Mahseredjian are with École Polytechnique de Montréal, Montreal, QC H3C 3A7, Canada (e-mail: ulas.karaagac@polymtl.ca; jean.mahseredjian@polymtl.ca).

S. O. Faried is with the University of Saskatchewan, Saskatoon, SK S7N 5A9, Canada (e-mail: sherif.faried@usask.ca).

A.-A. Edris is with Quanta Technology, Oakland, CA 94612 USA (e-mail: aedris@Quanta-technology.com).

Color versions of one or more of the figures in this paper are available online at http://ieeexplore.ieee.org.

Digital Object Identifier 10.1109/TSG.2014.2330453

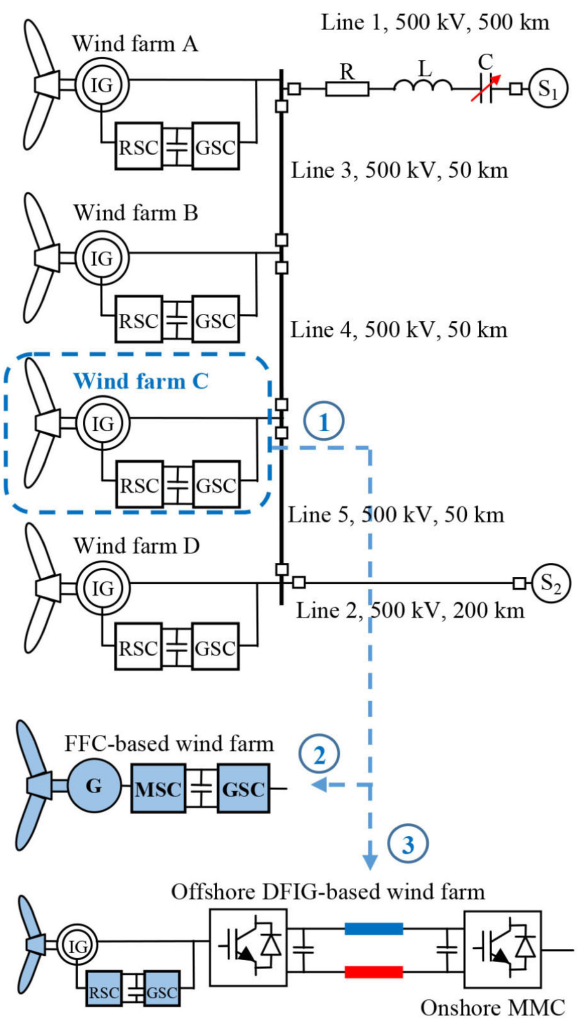

Fig. 1. Schematic diagram of the system under study.

A, B, C, and D that are connected in tandem by three, 500 kV, 50 km transmission lines. Moreover, wind farms A and D are connected to two large systems through two 500 kV transmission lines designated as lines 1 and 2. Line 2 is 200 km long while line 1 which is series capacitor compensated is 500 km long. In the investigations conducted in this paper, the following three scenarios are considered for wind farm C.

1) Wind farm C is a DFIG-based wind farm.
2) Wind farm C is a FFC-based wind farm.
3) Wind farm C is an offshore wind farm (OWF) consists of DFIG wind turbines and connected to the onshore ac grid through a MMC topology based voltage source converter (VSC) HVDC.

The compositions, ratings, operating wind speeds, and power outputs of the four wind farms are given in Table I. The medium voltage collector grid is represented with its equivalent PI circuit model [11]. The HVDC system includes two 401-level MMC terminals (± 110 kV, 150 MW) and a single-core 100 km submarine cable. The series capacitive compensation degrees of line 1 are selected within the practical range.

Faults are assumed to occur on line 2 near wind farm D and to be cleared by circuit breaker operations that leave the train of the four wind farms radially connected to the series capacitor compensated transmission line. This fault clearing scenario is similar to that of the Zorillo Gulf wind farm incidence.

TABLE I
WIND FARMS DATA

Wind farm	Rating, operating speed and output power
A	100 × 1.5 MW wind turbines, wind speed = 11 m/s, ≈ 142.5 MW
B, C	100 × 1.5 MW wind turbines, wind speed = 10 m/s, ≈ 110 MW
D	100 × 1.5 MW wind turbines, wind speed = 9 m/s, ≈ 75 MW
FFC wind farm	75 × 2 MW wind turbines, wind speed = 10 m/s, ≈ 110 MW
Offshore wind farm	100 × 1.5 MW DFIG wind turbines, wind speed = 10 m/s, ≈ 110 MW

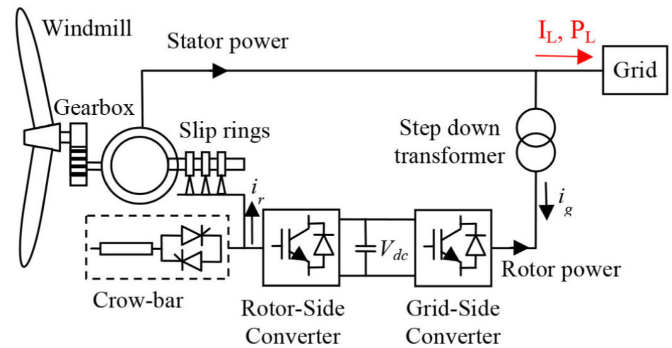

Fig. 2. Schematic diagram of a DFIG wind turbine.

III. WIND TURBINE MODELS AND CONTROL

A. DFIG-Based Wind Farm

The basic configuration of a DFIG wind turbine is shown in Fig. 2, where the stator of the induction machine is directly connected to the grid and the wound rotor is connected to the grid through a BtB link. The BtB link consists of two, three-phase pulse-width modulated (PWM) VSCs [rotor-side converter (RSC) and grid-side converter (GSC)] coupled to a common DC bus. A line inductor and an ac filter are used at the GSC to improve power quality. A crowbar is used as a backup protection device. Details of DFIG wind turbines mathematical modeling and control are given in [12].

The aggregated model of 1.5 MW, 60 Hz DFIG wind turbines in [13] is used in this paper. The model includes a pitch control to limit the maximum speed, a DC resistive chopper to limit the DC voltage and avoid the crowbar ignition during ac faults, a two-mass model to represent low frequency oscillations of the wind turbine drive system and over/under voltage protection. The DFIG converters are modeled with their average value models (AVMs) [13]–[16].

B. FFC-Based Wind Farm

The FFC concept uses a permanent-magnet synchronous generator (PMSG) connected to the grid through a BtB link. Depending on the size of the wind turbine, the PMSG side

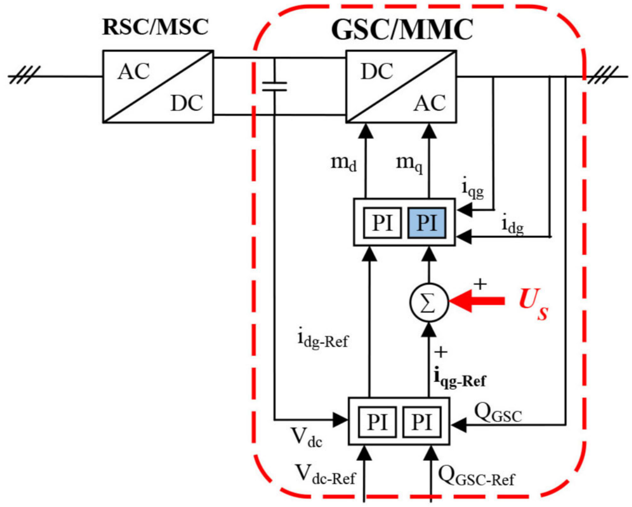

Fig. 3. Schematic diagram of a general control scheme of the GSC of a BtB converter incorporating a supplemental control signal.

converter (MSC) can be either a diode rectifier or a VSC. On the other hand, the GSC is typically a VSC. This paper considers the BtB VSC topology.

Similar to the DFIG, the control of the FFC is achieved by controlling the MSC and GSC [12]. The MSC controls the active power delivered by the PMSG, and follows a tracking characteristic to adjust the PMSG speed for optimal power generation depending on wind speed. The function of GSC is maintaining the DC bus voltage, i.e., transmitting the active power delivered to the DC link by the MSC. It is also used to control the reactive power delivered to the grid.

A generic 2 MW, 60 Hz FFC model is used in studies of this paper. The model includes a pitch control, DC chopper and over/under voltage protections. A two-mass model is used to represent the turbine drive system. The FFC converters are modeled with their AVMs.

C. Offshore Wind Farm

The OWF consists of an aggregated model of 1.5 MW, 60 Hz DFIG based wind turbines and connected to the onshore grid through a ± 110 kV, 150 MW MMC-HVDC system. The MMC topology considered in this paper is based on the preliminary design of a 401-level MMC-HVDC system planned to interconnect the 400 kV networks of France and Spain by 2013 [17]. The function of the offshore MMCs is to transmit the active power generated by the OWF and to set a voltage reference for the DFIGs. On the other hand, the function of onshore MMC is similar to the GSC of FFC wind turbine. It injects the active power transmitted by the offshore MMC to the onshore ac grid while maintaining the DC network voltage at desirable level. In addition, it supports the onshore ac grid voltage during steady-state operation and system faults [18]. The AVM-AVM combination of MMC and DFIG converters [13], [16] is used in this paper.

IV. Subsynchronous Interaction Damping Controller

SSI damping is achieved by adding a supplementary control signal in the reactive power control loop of the GSC (before the PI regulator of the inner control loop) of DFIG or FFC or HVDC onshore MMC as illustrated in Fig. 3. An *m*-stage lead-lag compensation based supplemental controller incorporating wash-out and band pass filters, shown in Fig. 4, is adopted for modulating the wind farm reactive power outputs for SSI damping.

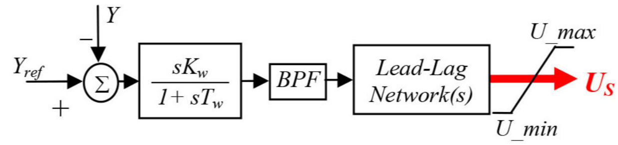

Fig. 4. Block diagram of a general lead-lag supplemental controller.

Although not shown in Fig. 3, the outer control loop of the reactive power control includes an ac voltage override block intended to maintain the ac voltage within acceptable limits. It should be noted that, such a control scheme is also essential for the desired fault ride through (FRT) capability. In order to avoid any possible detrimental effect of the SSR auxiliary control on the FRT capability of the wind farms, the SSR control signal (U_S in Fig. 3) is blocked when the override block is active due to low voltage at the wind turbine (or onshore MMC) ac terminals.

In scenario 1, the controller is considered to be installed on each wind turbine, and the wind turbine line current and real output power (I_L and P_L shown in Fig. 2) are selected as the inputs to the four wind farm supplemental controls. It should be noted that, the rotor speed contains, generally, high noise due to the torsional oscillations and is not suitable for this reason.

In scenario 2, there is only one central controller located in wind farm C and it accepts a remote input signal (either transmission line 1 current or power) and sends an output signal (U_S in Fig. 4) to each FFC-type wind turbine. In scenario 1, it is also feasible to use a similar central controller or to use those remote signals as input to the supplemental controller installed on each DFIG. However, these approaches require communication between each wind turbine and the central controller and/or the measuring point, hence are not considered in this paper. In scenario 3, a controller similar to that in scenario 2 is used to provide supplementary control signal to the reactive power control loop of the onshore MMC of the HVDC. Unlike scenario 1, only wind farm C accepts the supplementary control signal in scenarios 2 and 3. Moreover, it is assumed in scenarios 2 and 3 the availability of a wide-area network of synchronized phasor measurement units (PMUs) where measurement signals can be downloaded at the controller in real time without delay [19], [20].

In the case of the current input to the supplemental controller, the phase currents are transformed to the dq0 reference frame and the current magnitude is obtained as shown in Fig. 5. A trial-and-error approach is adopted in the investigations conducted in this paper for finding appropriate controller gains and time constants that result in an acceptable oscillations damping. The fine tuning of the parameters is then achieved by performing repetitive time-domain simulations to minimize the cost function

$$C = \int_{TC}^{TF} (\Delta Y')^2 dt \qquad (1)$$

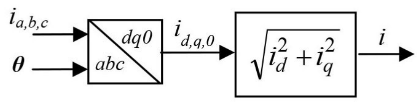

Fig. 5. Extracting the input transmission line current signal from its phase quantities.

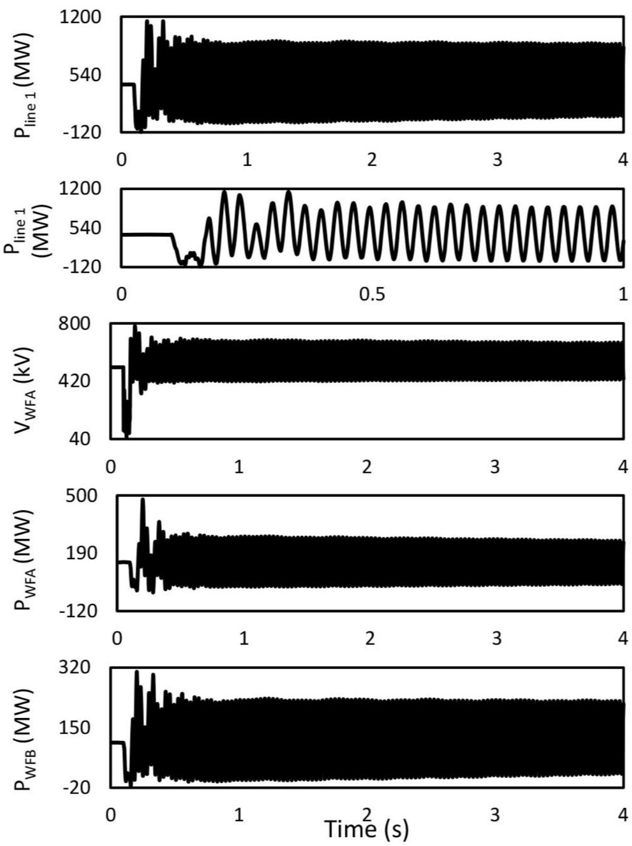

Fig. 6. Transient time responses of transmission line 1 real power, wind farm A terminal voltage and real output power, and wind farm B real output power during and after clearing a 3-cycle, three-phase fault on line 2 (supplemental controls are not activated).

where TC is the fault clearing time, TF is the total simulation time and $\Delta Y'$ is the output of the band pass filters in supplemental controller. The design of optimal supplemental controls using nonlinear control techniques, such as indirect adaptive control, is out of scope of this paper.

V. Analyzed Mitigation Scenarios and Time Domain Simulation Results

A. 50% Compensation Degree, Wind farm C is DFIG-Based Wind Farm

Fig. 6 illustrates the time responses of transmission line 1 real power flow, wind farm A terminal voltage and real output power as well as wind farm B real output power during and after clearing a 3-cycle, three-phase fault on line 2 for the case when the supplemental controls in the four wind farms are not in service. Figs. 7 and 8 show the corresponding time response when the supplemental controls are activated and the input signals are the wind turbine line current and real output power, respectively. Moreover, Fig. 9 shows wind farm A

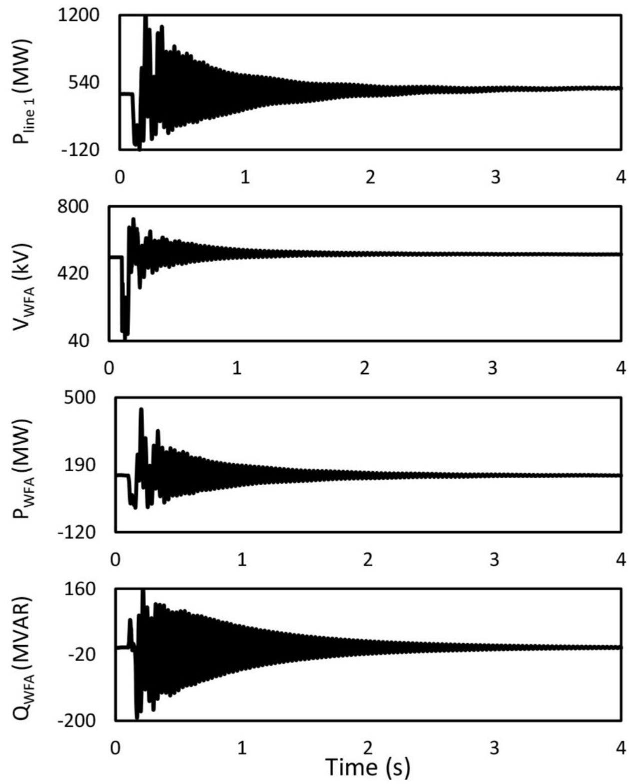

Fig. 7. Transmission line 1 real power, wind farm A terminal voltage and real and reactive output power responses to a 3-cycle three-phase fault on line 2 (supplemental controls are activated in all four wind farms, stabilizing signal is wind turbine line current).

supplemental control output signals U_S before and after the limiter of Fig. 4. It can be seen from Fig. 6 that, at this compensation degree, the two wind farms exhibit SSI (notice the sustained oscillations in the terminal voltage and real output power) with similar mechanism at a subsynchronous frequency of $60 - f_e$ = 31.32 Hz where f_e is the network resonance frequency in the stator currents [6]. This is also the case for wind farms C and D which their real output powers are not shown in Fig. 6. It is worth noting also that at 42% compensation degree, SSI does not occur as shown in Appendix A. The comparison between
Figs. 6–8 establishes the effectiveness of the supplemental control in mitigating SSI. It can also be concluded from Figs. 7 and 8 that both of the wind turbine line current and real output power reflect the SSI oscillations as they demonstrate of being effective control signals for SSI damping.

B. 55% Compensation Degree, Wind Farm C is Full-Scale Frequency Converter-Based Wind Farm

This case study confirms that FFC wind turbines are immune to SSI [21] and demonstrates the effectiveness of supplemental controls in the reactive power control loops of their GSC in damping SSI in nearby DFIG wind turbines.

Fig. 10 illustrates the time responses of transmission line 1 real power, wind farm A terminal voltage and real output power as well as the FFC wind farm (wind farm C) real output power during and after clearing a 3-cycle, three-phase fault on line 2 for the case when the supplemental control in wind

This article has been accepted for inclusion in a future issue of this journal. Content is final as presented, with the exception of pagination.

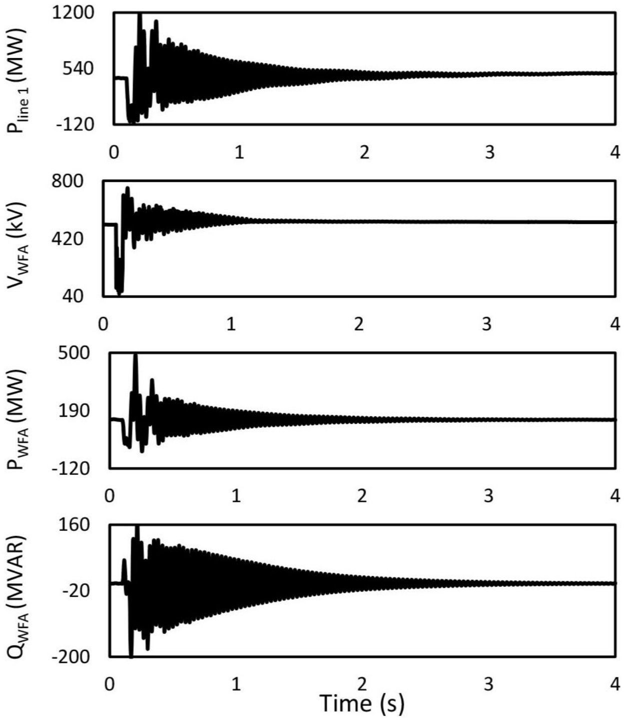

Fig. 8. Transient time responses of transmission line 1 real power, wind farm A terminal voltage and real and reactive output powers during and after clearing a 3-cycle three-phase fault on line 2 (supplemental controls are activated in all four wind farms, stabilizing signal is wind turbine real power).

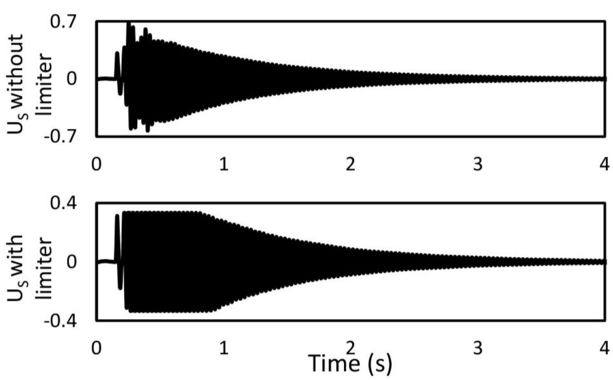

Fig. 9. Wind farm A supplemental control output signals U_S with and without the limiter during and after clearing a 3-cycle, three-phase fault on line 2 (supplemental controls are activated in all four wind farms, stabilizing signal is wind turbine line current).

farm C is not in service. Figs. 11 and 12 illustrate the corresponding time responses when the supplemental control is activated and the input signals are transmission line 1 current and real power flow, respectively.

As the result of the presence of the FFC wind farm that can be considered as a voltage controlled bus, SSI occurs in this case at a relatively higher compensation degree, namely 55% as it is shown in Fig. 10. As it can be seen from this figure, wind farm C real power output demonstrates no apparent susceptibility of the wind farm to SSI. The comparison between Fig. 10 and Figs. 11 and 12 establishes the effectiveness of wind farm C supplemental control in mitigating SSI. It can also be concluded from Figs. 11 and 12 that both of

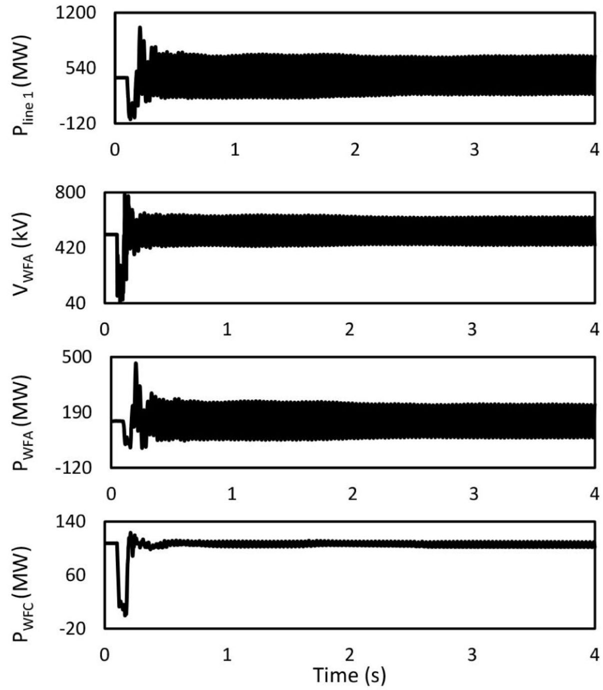

Fig. 10. Transient time responses of transmission line 1 real power, wind farm A terminal voltage and real power, and wind farm C real power during and after clearing a 3-cycle, three-phase fault on line 2 (supplemental control in wind farm C is not activated).

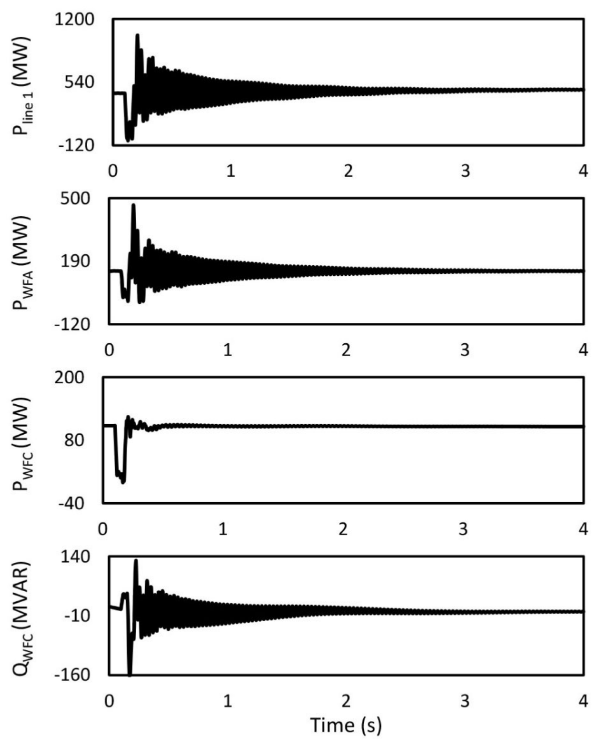

Fig. 11. Transient time responses of transmission line 1 real power, wind farm A real power, and wind farm C real and reactive powers during and after clearing a 3-cycle, three-phase fault on line 2 (supplemental control in wind farm C is activated, transmission line 1 current is the stabilizing signal).

transmission line 1 current and real power flow reflect the SSI oscillations as they demonstrate of being effective control signals for SSI damping.

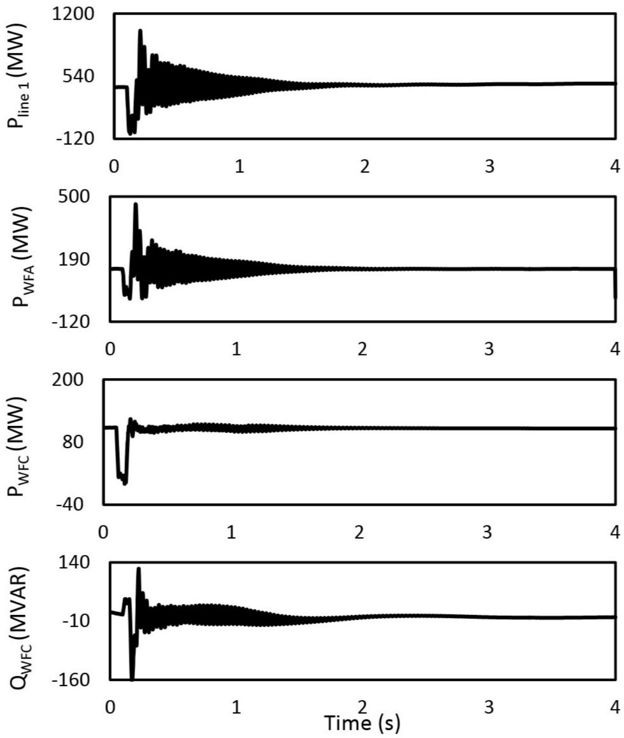

Fig. 12. Transient time responses of transmission line 1 real power, wind farm A real power, and wind farm C real and reactive powers during and after clearing a 3-cycle, three-phase fault on line 2 (supplemental control in wind farm C is activated, transmission line 1 real power flow is the stabilizing signal).

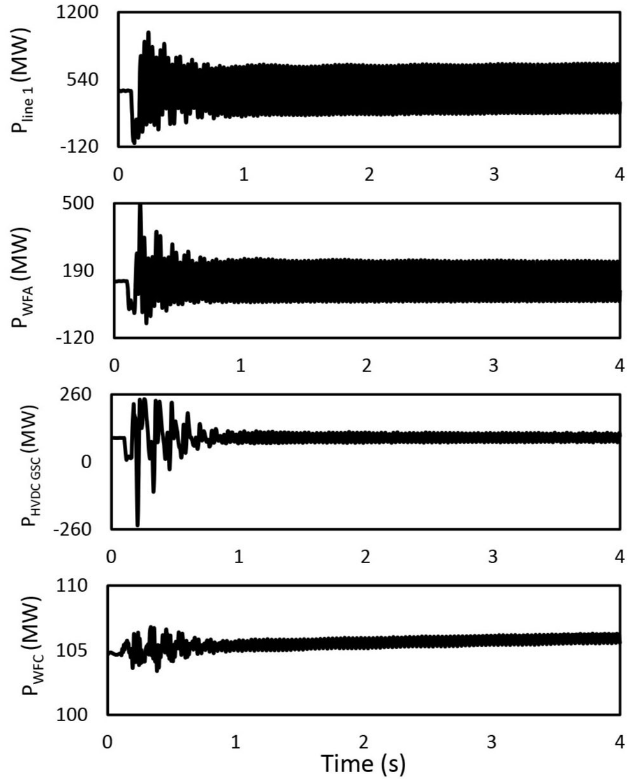

Fig. 13. Transient time responses of transmission line 1 real power, wind farms A and C real output power, and wind the real output power of the HVDC GSC during and after clearing a 3-cycle, three-phase fault on line 2 (supplemental control in wind farm C is not activated).

C. 55% Compensation Degree, Wind Farm C is Offshore DFIG-Based Wind Farm

Similar to Case B, this case study confirms that wind turbines connected to the grid through HVDC link are immune to SSI and demonstrates the effectiveness of supplemental controls in the reactive power control loop of the HVDC onshore MMC in damping SSI in nearby DFIG wind turbines. Here again, due to the presence of the HVDC link, SSI occurs at 55% compensation degree.

Fig. 13 illustrates the time responses of transmission line 1 real power flow, wind farms A and C real output powers as well as the real output power of the HVDC onshore MMC during and after clearing a 3-cycle, three-phase fault on line 2 for the case when the supplemental control in wind farm C is not in service. Fig. 14 illustrates the corresponding time responses when the supplemental control is activated and the input signal is transmission line 1 real power flow. Here again, the comparison between Figs. 13 and 14 demonstrates the effectiveness of wind farm C supplemental control in mitigating SSI in wind farms A, B, and D.

VI. Impact of Phase Imbalance Series Capacitive Compensation on SSI

An effective SSR countermeasure based on creating phase imbalance during system disturbances was introduced in the early nineties [22]–[24]. The idea behind phase imbalance which is accomplished using two LC resonant circuits with a resonance frequency of ω_o is weakening the electromechanical coupling which results in the reduction of the energy exchanged between the electrical network and the turbine generator shaft systems. In such a countermeasure illustrated in Fig. 15, in addition to the equal compensating capacitor banks on the three phases (C_{TOTAL}), two phases are modified by inserting in series with them two series resonant circuits L_a, C_a and L_b, C_b with ω_o is the resonance frequency. Thus, at the power frequency, the three phases have equal degree of capacitive compensation whereas at any other frequency they exhibit unequal capacitive compensation. The effectiveness of such a phase imbalance scheme in damping SSI in scenario A (50% compensation degree, wind farm C is a DFIG-based wind farm) is examined for the three combinations shown in Table II. The selection criterion for these combinations is that the values of C_a and C_b should not be much larger than C_{TOTAL}.

Figs. 16 and 17 show the transient time responses of transmission line 1 real power flow, wind farm A terminal voltage and real power as well as wind farm B real power with the phase imbalance scheme during and after clearing the same fault of Fig. 6 for cases I and II of Table II, respectively. It can be seen from the comparison between Figs. 6, 16, and 17 that the phase imbalance capacitive compensation schemes provide a significant damping to SSI that is comparable to that provided by the wind farm supplemental controls. As it can be seen from Fig. 17, the SSI is completely damped in less than 1 s. Moreover, the scheme limits the high transients during

This article has been accepted for inclusion in a future issue of this journal. Content is final as presented, with the exception of pagination.

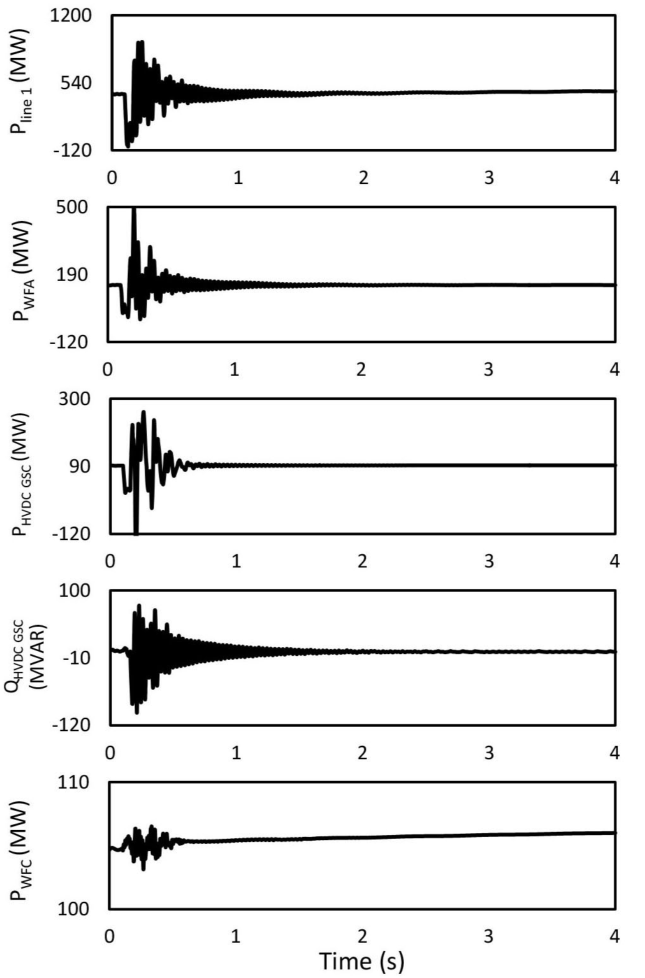

Fig. 14. Transient time responses of transmission line 1 real power, wind farms A and C real output power, and wind the HVDC GSC real and reactive powers during and after clearing a 3-cycle, three-phase fault on line 2 (supplemental control in wind farm C is activated, transmission line 1 real power flow is the stabilizing signal).

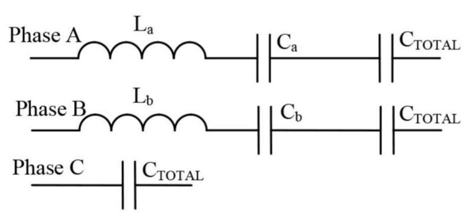

Fig. 15. Phase-imbalance series capacitive compensation scheme with two resonant circuits.

the fault and its clearing process. It is worth noting here that similar damping level is obtained from case III in Table II.

Fig. 18 shows the frequency spectrums (obtained using fast Fourier transform analysis) of wind farm A stator current for the study cases illustrated in Figs. 6 and 16 during the time interval between fault clearing and the time t = 2 s. As it can be seen from this figure, during SSI of Fig. 6, the network resonance frequency $f_e = 28.68$ Hz is clearly present in the frequency spectrum. It can also be seen from Fig. 18 that the phase imbalance series capacitive compensation scheme significantly attenuates this network resonance frequency.

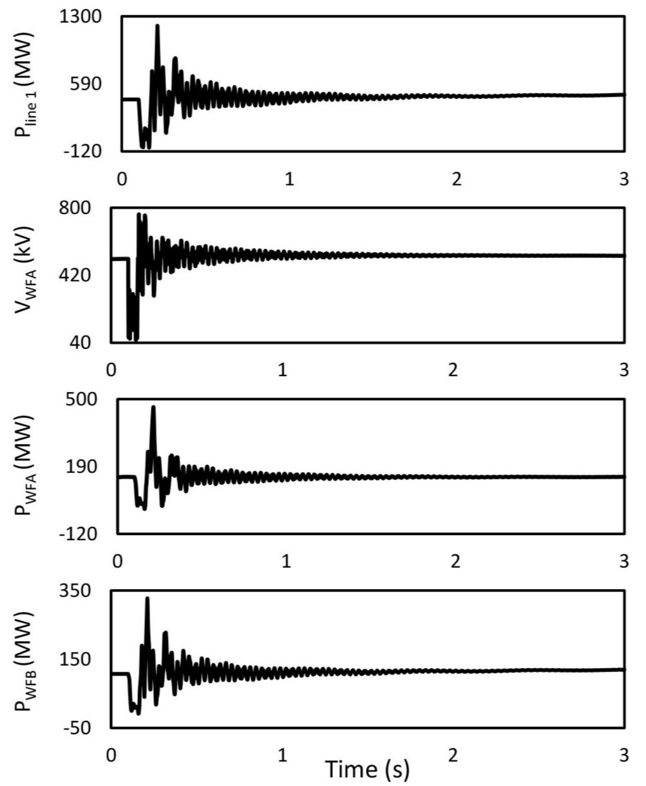

Fig. 16. Transient time responses of transmission line 1 real power, wind farm A terminal voltage and real power, and wind farm B real power during and after clearing a 3-cycle three-phase fault on line 2 (case I of phase imbalance series capacitive compensation).

TABLE II

THREE EXAMINED COMBINATIONS FOR THE RESONANT CIRCUITS

Case	C_{TOTAL}/C_a	C_{TOTAL}/C_b
I	0.25	0.5
II	0.5	1
III	0.58	0.93

As phase imbalance can also be created using a single resonant circuit as shown in Fig. 19, the transient time responses of transmission line 1 and wind farm A real power for such a case with $C_{TOTAL}/C_a = 0.5$ are shown in Fig. 20. As it can be seen from this figure, the new scheme of Fig. 19 also provides good damping to SSI.

VII. FUTURE RESEARCH

The extensions to the studies reported in this paper are as follows.

1) Robust design of the supplementary controller using constrained recursive least square algorithm and dynamic pole-shift technique [25]. An important aspect in the controller design is the time delay in computing the phasor quantities and the variable communication network latency for the controller to use remote synchrophasor data [26]–[27]. Such a controller, would include several phase compensators, each is designed for specific data latency. Based on the latency of the arriving synchrophasor data, the adaptive controller would select the proper compensator to use [28].

This article has been accepted for inclusion in a future issue of this journal. Content is final as presented, with the exception of pagination.

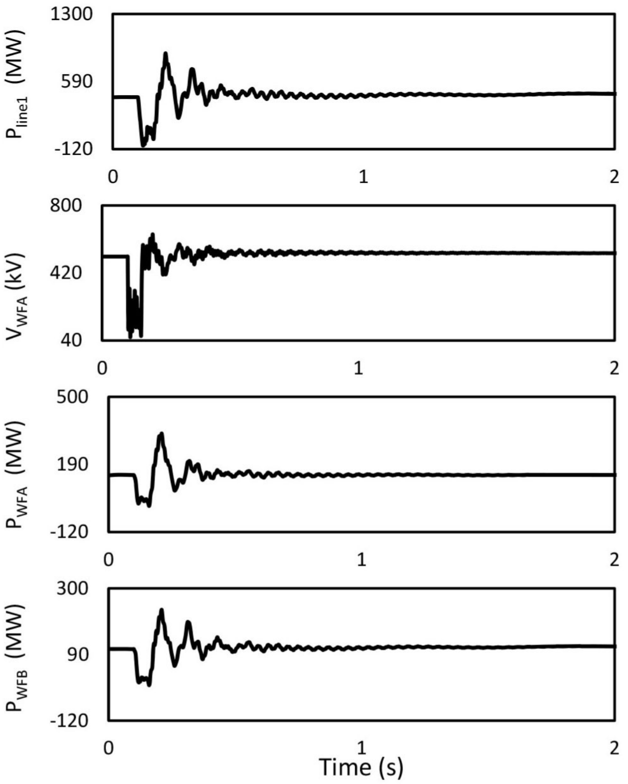

Fig. 17. Transient time responses of transmission line 1 real power, wind farm A terminal voltage and real power, and wind farm B real power during and after clearing a 3-cycle three-phase fault on line 2 (case II of phase imbalance series capacitive compensation).

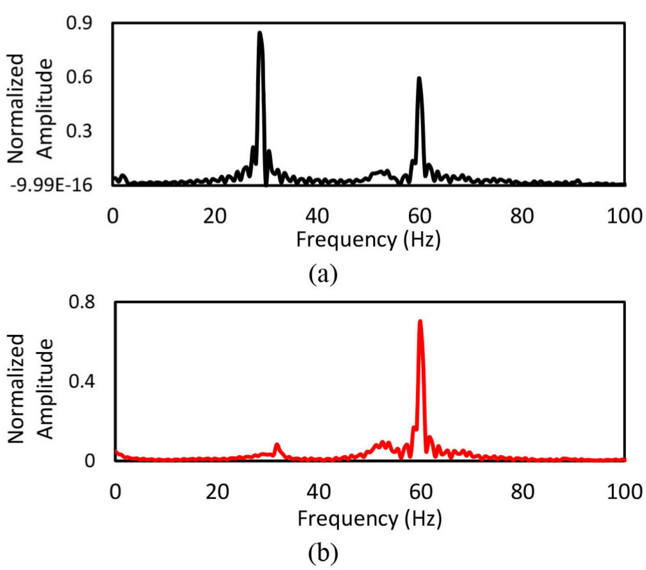

Fig. 18. Frequency spectrums of wind farm A stator current during the time interval between fault clearing and t = 2 s. (a) Without phase imbalance. (b) With case I of phase imbalance.

2) The expansion of the study system of Fig. 1 to incorporate a large turbine-generator connected to a large system through a second series capacitor compensated transmission line. Such a modified system would allow investigating the use of the presented supplemental controls and phase-imbalance series capacitive compensation schemes in simultaneous mitigation of SSI and SSR oscillations in the turbine-generator shaft system.

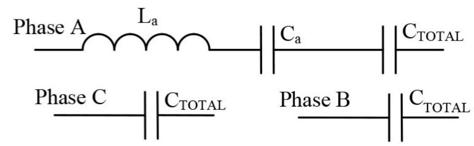

Fig. 19. Phase-imbalance series capacitive compensation scheme with one resonant circuit.

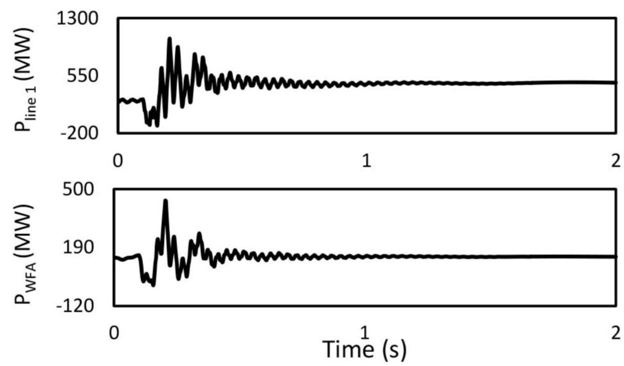

Fig. 20. Transient time responses of transmission line 1 real power and wind farm A real power during and after clearing a 3-cycle three-phase fault on line 2 (phase imbalance series capacitive compensation in one phase with $C_{TOTAL}/C_a = 0.5$).

VIII. Conclusion

This paper has used detailed models for DFIG and FFC wind turbines as well as offshore wind turbines connected to the grid through MMC HVDC links to capture the SSI phenomenon between DFIG-based wind farms and series capacitor compensated transmission systems. Contrary to the reported studies that have used simplified DFIG wind turbine-models and have failed to capture SSI at 50%, 60%, or even 70% compensation degrees, the models used in the investigations of this paper have captured SSI at the practical compensation degrees (considering the fact that the Zorillo Gulf wind farm incident occurred at 50% compensation degree).

The paper has also proposed methods for damping SSI between DFIG-based wind farms and series capacitor compensated transmission systems for a number of wind farm scenarios. SSI damping is achieved by modulating the reactive power of the GSCs of DFIG, FFC wind turbines and the HVDC onshore MMC of offshore wind farms using supplemental controls. The effectiveness of the various supplemental controls in damping SSI is validated through time-domain simulation studies on a test system. Moreover, the results of studies carried out to explore the impact of phase imbalance series capacitive compensation schemes on SSI damping show that, for the system under study, such schemes provide damping comparable to that provided by the proposed supplemental controls.

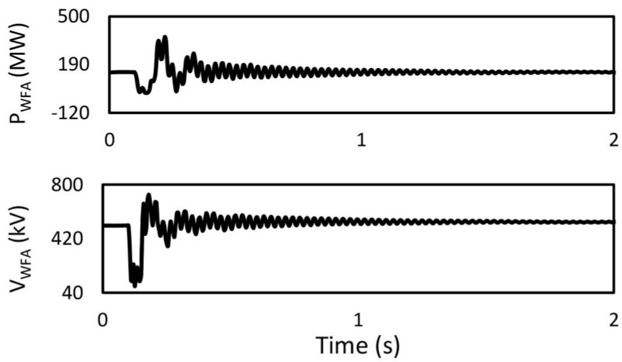

Fig. 21. Transient time responses of wind farm A real power and terminal voltage during and after clearing a 3-cycle, three-phase fault on line 2 (42% compensation degree, supplemental controls are not activated).

TABLE III
SSI CONTROLLER PARAMETERS

Block	Transfer function
Washout filter	$\frac{0.1s}{1+0.1s}$
Band-pass filter (BPF)	$\frac{62.83s}{s^2+62.83s+35500}$
Lead-lag network	$\frac{0.05(s+2500)}{s+1}$
U max, U min	0.333, -0.333

APPENDIX A

Fig. 21 illustrates the time responses of wind farm A real output power and terminal voltage during and after clearing a 3-cycle, three-phase fault on line 2 for Scenario 1 when the supplemental controls in the four wind farms are not in service and Line 1 compensation degree is 42%. As it can be seen from this figure, the oscillations in the real power and terminal voltages are damped indicating the absence of SSI. It is worth noting here that this is also the case at 45% compensation degree but the damping is less than that at 42%. SSI exists at 46% compensation degree.

APPENDIX B

SAMPLE OF THE SUPPLEMENTAL CONTROLLER PARAMETERS

Due to space limitations, the supplemental controller parameters, shown in Table III for scenario 1 (stabilizing signal is the wind turbine line current) are only given.

REFERENCES

[1] L. Fan, R. Kavasseri, Z. Lee Miao, and C. Zhu, "Modeling of DFIG-based wind farms for SSR analysis," *IEEE Trans. Power Del.*, vol. 25, no. 4, pp. 2073–2082, Oct. 2010.

[2] A. Ostadi, A. Yazdani, and R. Varma, "Modeling and stability analysis of a DFIG-based wind-power generator interfaced with a series-compensated line," *IEEE Trans. Power Del.*, vol. 24, no. 3, pp. 1504–1514, Jul. 2009.

[3] L. C. Gross, "Sub-synchronous grid conditions: New event, new problem, and new solutions," in *Proc. 37th Annu. Western Protective Relay Conf.*, Spokane, WA, USA, Oct. 2010, pp. 1–19.

[4] G. D. Irwin, A. K. Jindal, and A. L. Isaacs, "Sub-synchronous control interactions between Type 3 wind turbines and series compensated AC transmission systems," in *Proc. PES Gen. Meet.*, Detroit, MI, USA, Jul. 2011, pp. 1–6.

[5] NERC. (2011, Jul. 26). "Lesson learned—Sub-synchronous interaction between series-compensated transmission lines and generation," Online Rep. Lesson Learned#: 20110705 [Online]. Available: http://www.nerc.com/files/LL_45_Sub-Synchronous_Interaction.pdf

[6] D. H. R. Suriyaarachchi *et al.*, "Application of an SVC to damp sub-synchronous interaction between wind farms and series compensated transmission lines," in *Proc. IEEE PES Gen. Meet.*, San Diego, CA, USA, Jul. 2012, pp. 1–6.

[7] L. Fan and Z. Miao, "Mitigating SSR using DFIG-based wind generation," *IEEE Trans. Sustain. Energy*, vol. 3, no. 3, pp. 349–358, Jul. 2012.

[8] B. Badrzadeh, M. Sahni, D. Muthumuni, Y. Zhou, and A. Gole, "Sub-synchronous interaction in wind power plants—Part I: Study tools and techniques," in *Proc. IEEE PES Gen. Meet.*, San Diego, CA, USA, Jul. 2012, pp. 1–9.

[9] J. Adams, V. A. Pappu, and A. Dixit, "ECORT experience screening for sub-synchronous control interaction in the vicinity of series capacitor banks," in *Proc. IEEE PES Gen. Meet.*, San Diego, CA, USA, Jul. 2012, pp. 1–5.

[10] D. H. R. Suriyaarachchi, U. D. Annakkage, C. Karawita, and D. A. Jacobson, "A procedure to study sub-synchronous interactions in wind integrated power systems," *IEEE Trans. Power Syst.*, vol. 28, no. 1, pp. 377–384, Feb. 2013.

[11] E. Muljadi *et al.*, "Equivalencing the collector system of a large wind power plant," in *Proc. IEEE PES Gen. Meet.*, Montreal, QC, Canada, Jun. 2006, pp. 1–9.

[12] O. Anaya-Lara, N. Jenkins, J. Ekanayake, P. Cartwright, and M. Hughes, *Wind Energy Generation: Modelling and Control*. Hoboken, NJ, USA: Wiley, 2009.

[13] J. Peralta *et al.*, "Dynamic modeling of MMC-based MTDC systems for the integration of offshore wind generation," in *Proc. CIGRE Canada Conf. Power Syst.*, Montreal, QC, Canada, Sep. 2012, pp. 1–12.

[14] J. Morren *et al.*, "Comparison of complete and reduced models of a wind turbine with doubly-fed induction generator," in *Proc. 10th European Conf. Power Electron. Appl.*, Toulouse, France, Sep. 2003, pp. 1–10.

[15] J. G. Slootweg, H. Polinder, and W. L. Kling, "Representing wind turbine electrical generating systems in fundamental frequency simulations," *IEEE Trans. Energy Convers.*, vol. 18, no. 4, pp. 516–524, Dec. 2003.

[16] U. Karaagac, H. Saad, J. Mahseredjian, S. Jensen, and L. Cai, "Off-shore wind power plant modeling precision and efficiency in electromagnetic transient simulation programs," in *Proc. 11th Int. Workshop Large-Scale Integr. Wind Power Power Syst.*, Lisbon, Portugal, Nov. 2012, pp. 1–6.

[17] J. Peralta, H. Saad, S. Dennetière, J. Mahseredjian, and S. Nguefeu, "Detailed and averaged models for a 401-level MMC-HVDC system," *IEEE Trans. Power Del.*, vol. 27, no. 3, pp. 1501–1508, Jul. 2012.

[18] U. Karaagac, H. Saad, J. Mahseredjian, S. Jensen, and L. Cai, "Examination of fault ride-through methods for off-shore wind farms connected to the grid through VSC-based HVDC transmission," in *Proc. 11th Int. Workshop Large-Scale Integr. Wind Power Power Syst.*, Lisbon, Portugal, Nov. 2012, pp. 1–6.

[19] B. Bhargava and A. Salazar, "Use of synchronized phasor measurement system for monitoring power system stability and system dynamics in real-time," in *Proc. 2008 IEEE Power Energy Soc. Gen. Meet.*, Pittsburgh, PA, USA, pp. 1–8.

[20] X. Xie, J. Xiao, C. Lu, and Y. Han, "Wide-area stability control for damping interarea oscillations of interconnected power systems," *IEE Proc. Gener. Transm. Distrib.*, vol. 153, no. 5, pp. 507–514, Sep. 2006.

[21] H. T. Ma, P. B. Brogan, K. H. Jensen, and R. J. Nelson, "Sub-synchronous control interaction studies between full-converter wind turbines and series-compensated AC transmission lines," in *Proc. PES Gen. Meet.*, San Diego, CA, USA, Jul. 2012, pp. 1–5.

[22] A. Edris, "Series compensation schemes reducing the potential of subsynchronous resonance," *IEEE Trans. Power Syst.*, vol. 5, no. 1, pp. 219–226, Feb. 1990.

[23] A. Edris, "Subsynchronous resonance countermeasure using phase imbalance," *IEEE Trans. Power Syst.*, vol. 8, no. 4, pp. 1438–1447, Nov. 1993.

[24] M. R. Iravani and A. Edris, "Eigen analysis of series compensation schemes reducing the potential of subsynchronous resonance," *IEEE Trans. Power Syst.*, vol. 10, no. 2, pp. 876–883, May 1995.

[25] D. Rai, R. Gokaraju, and S. O. Faried, "Adaptive control using constrained RLS and dynamic pole-shift technique for TCSCs," *IEEE Trans. Power Del.*, vol. 29, no. 1, pp. 224–234, Feb. 2014.
[26] J. H. Chow and S. Ghiocel, "An adaptive wide-area power system damping controller using synchrophasor data," in *Control and Optimization Theory for Electric Smart Grids*, A. Chakrabortty and M. D. Ilić, Eds. New York, NY, USA: Springer, 2012.
[27] B. Chaudhuri, R. Majumder, and B. C. Pal, "Wide-area measurement-based stabilizing control of power system considering signal transmission delay," *IEEE Trans. Power Syst.*, vol. 19, no. 4, pp. 1971–1979, Nov. 2004.
[28] D. Dotta, A. S. e Silva, and I. C. Decker, "Wide-area measurements-based two-level control design considering signal transmission delay," *IEEE Trans. Power Syst.*, vol. 24, no. 1, pp. 208–216, Feb. 2009.

Ulas Karaagac (M'08) received the M.S. and B.S. degrees in electrical and electronic engineering from Middle East Technical University, Ankara, Turkey, in 1999 and 2002, respectively, and the Ph.D. degree in electrical engineering from École Polytechnique de Montreal, Montreal, QC, Canada, in 2012.

He was a Research and Development Power Engineer with the Information Technology and Electronics Research Institute, Scientific and Technical Research Council of Turkey, Ankara, from 1999 to 2007. He is currently a Post-Doctoral Fellow at École Polytechnique de Montreal. His current research interests include modeling and simulation of large-scale power systems.

Sherif O. Faried (S'88–M'88–SM'00) received the B.Sc. and M.Sc. degrees from Ain Shams University, Cairo, Egypt, in 1979 and 1984, respectively, and the M.Sc. and Ph.D. degrees from the University of Saskatchewan, Saskatoon, SK, Canada, in 1988 and 1993, respectively, all in electrical engineering.

He is currently a Professor of Electrical Engineering with the Department of Electrical and Computer Engineering, University of Saskatchewan.

Jean Mahseredjian (F'13) received the M.A.Sc. and Ph.D. degrees from École Polytechnique de Montreal, Montreal, QC, Canada, in 1985 and 1991, respectively.

From 1987 to 2004, he was with IREQ (Hydro-Quebec), Varennes, QC, researching research and development activities related to the simulation and analysis of electromagnetic transients. In 2004, he joined the faculty of Electrical Engineering at École Polytechnique de Montreal, where he is currently a Professor.

Abdel-Aty (Aty) Edris (F'12) was born in Cairo, Egypt. He received the B.S. (Hons.) degree from Cairo University, Giza, Egypt; the M.S. degree from Ain-Shams University, Cairo; and the Ph.D. degree from the Chalmers University of Technology, Goteborg, Sweden.

He spent 12 years with ABB Company in Sweden and USA, researching the development and application of reactive power compensators and high voltage dc transmission systems. From 1992 to 2008, he was with the Electric Power Research Institute as the Manager of Flexible AC Transmission System Technology and as a Senior Technology Manager of EPRI Power Delivery and Markets. He is currently a Senior Director and an Executive Advisor at Quanta Technology.